

# Resistivity scaling model for metals with conduction band anisotropy

Miguel De Clercq,<sup>1</sup> Kristof Moors,<sup>2,\*</sup> Kiroubanand Sankaran,<sup>3</sup> Geoffrey Pourtois,<sup>3</sup>  
Shibesh Dutta,<sup>3,4</sup> Christoph Adelman,<sup>3</sup> Wim Magnus,<sup>3,1</sup> and Bart Sorée<sup>3,1,5</sup>

<sup>1</sup>*University of Antwerp, Physics Department, Groenenborgerlaan 171, B-2020 Antwerpen, Belgium*

<sup>2</sup>*University of Luxembourg, Physics and Materials Science Research Unit,  
Avenue de la Faïencerie 162a, L-1511 Luxembourg, Luxembourg*

<sup>3</sup>*imec, Kapeldreef 75, B-3001 Leuven, Belgium*

<sup>4</sup>*KU Leuven, Department of Physics and Astronomy, Celestijnenlaan 200D, B-3001 Leuven, Belgium*

<sup>5</sup>*KU Leuven, Electrical Engineering (ESAT) Department,  
Kasteelpark Arenberg 10, B-3001 Leuven, Belgium*

(Dated: December 14, 2024)

It is generally understood that the resistivity of metal thin films scales with film thickness mainly due to grain boundary and boundary surface scattering. Recently, several experiments and *ab initio* simulations have demonstrated the impact of crystal orientation on resistivity scaling. The crystal orientation cannot be captured by the commonly used resistivity scaling models and a qualitative understanding of its impact is currently lacking. In this work, we derive a resistivity scaling model that captures grain boundary and boundary surface scattering as well as the anisotropy of the band structure. The model is applied to Cu and Ru thin films, whose conduction bands are (quasi-)isotropic and anisotropic respectively. After calibrating the anisotropy with *ab initio* simulations, the resistivity scaling models are compared to experimental resistivity data and a renormalization of the fitted grain boundary reflection coefficient can be identified for textured Ru.

## I. INTRODUCTION

Many semiclassical and quantum mechanical resistivity scaling models (see [1–12]) have been developed over the last decades and have provided a satisfactory description for the thickness dependent resistivity of metal thin films down to nanometer scale thicknesses [13–18]. The thickness dependence can mainly be attributed to grain boundary and boundary surface scattering, whose impact on the resistivity increases when the film thickness is reduced. For grain boundaries, this is a consequence of the typical observation that grain sizes in polycrystalline films decrease with decreasing thickness.

Fuchs and Sondheimer developed a seminal semiclassical model that describes the impact of thin film boundary surface scattering on the resistivity by applying diffuse or partially diffuse boundary conditions [1, 2]. Mayadas and Shatzkes later included the impact of grain boundary scattering without invoking Matthiessen’s rule [3]. The resulting expression is still widely used today as it provides an analytical expression of the thin film resistivity as a function of its thickness, allowing for a straightforward analysis of experimental resistivity data and determining the relative impact of grain and film boundaries. The model is typically being considered with two fitting parameters that respectively represent the average reflection coefficient of the grain boundaries and the specularity of the thin film boundary surfaces (due to e.g. atomic-scale boundary roughness). In this way, the relative contribution of grain boundary and boundary surface scattering for the resistivity degradation can easily be read from the fitting parameters.

The Mayadas-Shatzkes model shines through its simplicity and wide applicability, but it is derived within the framework of the simplest effective mass description for the conduction bands. This offers a reasonable description in case the metal is nearly isotropic. However, it is not necessarily adequate for many metals in the periodic table whose band structure deviates significantly from an isotropic band structure, e.g. exhibiting an anisotropic Fermi velocity and multiple bands with multiple electron or hole pockets centered around different symmetry points in the Brillouin zone (e.g. Co, W, Os, Ru, Ir) [19, 20]. Particularly for textured thin films (see [21]) or nanowires that are grown along a specific crystal orientation [22–25], one can doubt the validity of this approach.

Recently, Li *et al.* proposed a phenomenological correction to the Fuchs-Sondheimer model for metal thin films of Os with a nonspherical Fermi surface to explain the experimental findings [26]. In this work, we derive a model to describe resistivity scaling of imperfect metal thin films, while retaining some features of the electronic structure to capture the impact of conduction band anisotropy. The model is similar in spirit to the Mayadas-Shatzkes model and provides the resistivity as a function of the film thickness in a straightforward manner with two fitting parameters representing grain boundary and film boundary surface scattering. The main extension of our model is the consideration of a diagonal effective mass tensor that is tailored for the metal and thin film texture under consideration.

The model is presented in section II after briefly reviewing the Mayadas-Shatzkes model, followed by a subsection on the effective mass fitting procedure. Section IV contains a discussion of the results, implications for experiments and limitations of applicability of the model. We conclude in section V.

\* E-mail: kristof.moors@uni.lu

## II. MODEL

The conduction electrons of a thin film, with length  $L$  along the transport direction, are modeled as quasi-free fermions residing in a single conduction band and being treated in the effective mass approximation. The film thickness is considered to be large enough such that the allowed three-dimensional wave vectors  $\mathbf{k}$ , providing a unique (apart from the two-fold spin degeneracy) label for the different electron states, can safely be assumed to be quasi-continuous.

### A. Mayadas-Shatzkes model

Mayadas and Shatzkes proposed a model for the resistivity scaling of polycrystalline films with reduced thicknesses due to an increase of grain boundary and boundary surface scattering [3]. The grain boundaries are modeled by a sequence of delta-function potential barriers normal to the transport direction  $x$ :

$$V^{\text{GB}} \equiv \sum_{i=1}^N S \delta(x - x_i). \quad (1)$$

We consider  $N$  barriers, leading to an average grain boundary separation  $d = L/N$ . The parameter  $d$  can be understood as the mean linear intercept for a random straight trajectory through a thin film sample along the transport direction, which can easily be extracted from plan-view TEM images for example [21, 27]. The barrier positions  $x_i$  are considered to be distributed according to a Gaussian distribution function  $g(x_1, \dots, x_N)$ ,

$$g(x_1, \dots, x_N) \equiv \frac{1}{L} \prod_{i=1}^{N-1} \frac{\exp[-(x_{i+1} - x_i - d)^2 / (2s^2)]}{(2\pi s^2)^{1/2}}, \quad (2)$$

with standard deviation  $s$  for the mean linear intercept. The Boltzmann transport equation is then considered to compute the distribution function  $f(\mathbf{k})$ . Keeping only the lowest-order contributions and assuming a small constant electric field vector  $\mathbf{E}$  oriented along the transport direction, the stationary Boltzmann equation reduces to

$$\begin{aligned} & eE v_x(\mathbf{k}) \frac{\partial f^{\text{eq}}(\epsilon(\mathbf{k}))}{\partial \epsilon} \\ &= \sum_{\mathbf{k}'} P(\mathbf{k}, \mathbf{k}') [f_1(\mathbf{k}') - f_1(\mathbf{k})] - \frac{f_1(\mathbf{k})}{\tau(\mathbf{k})}, \end{aligned} \quad (3)$$

where  $e$  is the electron charge,  $\epsilon(\mathbf{k})$  the electron state energy,  $v_x(\mathbf{k})$  the  $x$ -component of the electron velocity,  $\tau(\mathbf{k})$  the bulk collision time due to impurities, defects and electron-phonon interactions,  $P(\mathbf{k}, \mathbf{k}')$  the scattering rate to go from  $\mathbf{k}$  to  $\mathbf{k}'$  (or the opposite) as a result of elastic grain boundary scattering and  $f_1(\mathbf{k}) \equiv f(\mathbf{k}) - f^{\text{eq}}(\epsilon(\mathbf{k}))$  with  $f^{\text{eq}}(\epsilon(\mathbf{k}))$  the Fermi-Dirac distribution. Scattering at boundary surfaces is not yet included in this equation.

The scattering rates are calculated with Fermi's golden rule and an averaging over the distribution  $g(x_1, \dots, x_N)$ , leading to

$$\begin{aligned} P(\mathbf{k}, \mathbf{k}') &= F(|k_x|) \delta_{\mathbf{k}_\perp, \mathbf{k}'_\perp} \delta_{k_x, -k'_x}, \\ F(|k_x|) &\equiv \frac{\hbar k_F^2}{m_e |k_x| d} \frac{R}{1 - R} \\ &\times \frac{1 - \exp(-4k_x^2 s^2)}{1 + \exp(-4k_x^2 s^2) - 2 \exp(-k_x^2 s^2) \cos(2k_x d)}, \\ R &= 1 / [1 + \hbar^4 k_F^2 / (m_e S)^2], \quad \mathbf{k}_\perp \equiv (k_y, k_z). \end{aligned} \quad (4)$$

The derivation can be found in Appendix A. The reflection coefficient  $R$  for an electron at the Fermi level with wave vector perpendicularly oriented to a delta-function barrier was used to rewrite the transition probability. Note that the expression on the second line is corrected with a factor of two in comparison with Mayadas and Shatzkes. The solution of Eq. (3) is then given by

$$\begin{aligned} f_1(\mathbf{k}) &= -\tau^*(\mathbf{k}) eE v_x(\mathbf{k}) \frac{\partial f^{\text{eq}}(\epsilon(\mathbf{k}))}{\partial \epsilon}, \\ 1/\tau^*(\mathbf{k}) &\equiv 1/\tau(\mathbf{k}) + 2F(|k_x|). \end{aligned} \quad (5)$$

For random grain boundary configurations of typical metallic thin films, it is safe to assume  $k_F^2 s^2 \gg 1$ , such that  $F(|k_x|)$  reduces to

$$F(|k_x|) = \frac{\hbar k_F^2}{m_e |k_x| d} \frac{R}{1 - R}. \quad (6)$$

The conductivity  $\sigma_x^{\text{GB}}$  (along transport direction  $x$ ), taking into account the bulk scattering contribution and grain boundary scattering, can be calculated using [28, 29]:

$$\sigma_x^{\text{GB}} = -2e^2 \int \frac{d^3 k}{(2\pi)^3} v_x^2(\mathbf{k}) \tau^*(\mathbf{k}) \frac{\partial f^{\text{eq}}(\epsilon(\mathbf{k}))}{\partial \epsilon}. \quad (7)$$

The result obtained by Mayadas and Shatzkes, assuming zero temperature (being a very reasonable assumption for typical metals at room temperature) and an isotropic bulk collision time  $\tau$  (or equivalently an isotropic mean free path  $l_0$ ), is given by

$$\begin{aligned} \sigma^{\text{GB}}(\alpha) &= \frac{n_e e^2 \tau}{m_e} 3 \left[ \frac{1}{3} - \frac{\alpha}{2} + \alpha^2 - \alpha^3 \ln \left( \frac{1 + \alpha}{\alpha} \right) \right], \\ n_e &= k_F^3 / (3\pi^2) = (2m_e E_F)^{3/2} / (3\pi^2 \hbar^3), \\ \alpha &\equiv 2\tau \frac{\hbar k_F}{m_e d} \frac{R}{1 - R} = \frac{l_0}{d} \frac{2R}{1 - R}, \quad l_0 \equiv v_F \tau, \end{aligned} \quad (8)$$

with  $n_e$  the bulk electron density and  $v_F$  the Fermi velocity:  $v_F \equiv \hbar k_F / m_e$ . Scattering at the thin film boundary surfaces is not taken into account through a scattering probability, but through boundary conditions on the Boltzmann distribution function, carrying an additional dependence on the coordinate  $z$  normal to the film boundary surfaces. This approach was first introduced

by Fuchs and Sondheimer without the inclusion of grain boundary scattering [1, 2]. The Boltzmann equation becomes

$$\begin{aligned} v_z(\mathbf{k}) \frac{\partial f_1(z, \mathbf{k})}{\partial z} + eE v_x(\mathbf{k}) \frac{\partial f^{\text{eq}}(\epsilon(\mathbf{k}))}{\partial \epsilon} &= -\frac{f_1(z, \mathbf{k})}{\tau^*(\mathbf{k})}, \\ f_1(0, k_x, k_y, k_z) &= p f_1(0, k_x, k_y, -k_z) \quad (v_z(\mathbf{k}) > 0), \\ f_1(t, k_x, k_y, k_z) &= p f_1(t, k_x, k_y, -k_z) \quad (v_z(\mathbf{k}) < 0), \end{aligned} \quad (9)$$

where  $t$  is the film thickness  $p$  reflects the probability to scatter specularly at the boundary surfaces at  $z = 0$  and  $z = t$ , while diffuse scattering occurs with a probability  $1 - p$ . Note that the notion of a transverse velocity  $v_z(\mathbf{k})$  is invalid for extremely thin films, where confinement heavily affects the band structure. Due to the large conduction electron density of typical metals, this region

is limited to thin films with thicknesses up to a few atom layers, i.e.  $\sim 1$  nm [21, 30]. The solution of the equation with surface scattering boundary conditions is given by

$$\begin{aligned} f_1(z, \mathbf{k}) &= -\tau^*(\mathbf{k}) eE v_x(\mathbf{k}) \frac{\partial f^{\text{eq}}(\epsilon(\mathbf{k}))}{\partial \epsilon} F_p(z, \mathbf{k}), \\ F_p(z, \mathbf{k}) &\equiv 1 - \vartheta(k_z) \frac{(1-p) \exp\{-z/[\tau^*(\mathbf{k})v_z(\mathbf{k})]\}}{1-p \exp\{-t/[\tau^*(\mathbf{k})v_z(\mathbf{k})]\}} \\ &\quad - \vartheta(-k_z) \frac{(1-p) \exp\{(t-z)/[\tau^*(\mathbf{k})v_z(\mathbf{k})]\}}{1-p \exp\{t/[\tau^*(\mathbf{k})v_z(\mathbf{k})]\}}, \end{aligned} \quad (10)$$

with the Heaviside step function  $\vartheta(k)$  and Fuchs fraction  $F_p(z, \mathbf{k})$  (see Fig. 1). This solution leads to the following conductivity formula for thin films with grain boundary and partially diffusive boundary surface scattering on top of isotropic bulk collisions,  $\sigma^{\text{GB+BS}}(\alpha, p)$ :

$$\sigma^{\text{GB+BS}}(\alpha, p) = \sigma^{\text{GB}}(\alpha) - \frac{n_e e^2 \tau}{m_e} \frac{6}{\pi \kappa} (1-p) \int_0^{\pi/2} d\theta \int_0^{\pi/2} d\phi \frac{\sin^3 \theta \cos \theta \cos^2 \phi}{H^2(\alpha, \theta, \phi)} \frac{1 - \exp[-\kappa H(\alpha, \theta, \phi)/\cos \theta]}{1 - p \exp[-\kappa H(\alpha, \theta, \phi)/\cos \theta]}, \quad (11)$$

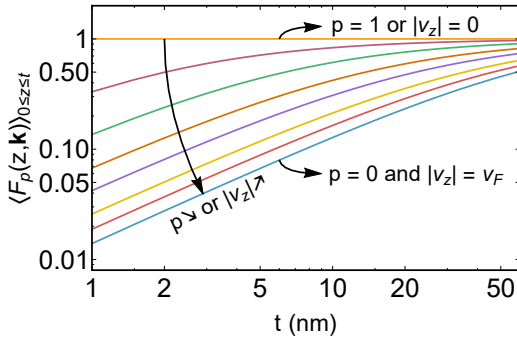


FIG. 1. The Fuchs fraction  $F_p(z, \mathbf{k})$ , defined in Eq. (10), is evaluated as a function of the film thickness  $t$ , showing its average over the position normal to the film boundaries for the full range of specularity parameters  $p$  ( $0 \leq p \leq 1$ ) and transverse velocities  $v_z$  ( $-v_F \leq v_z \leq v_F$ ). The bulk limit is retrieved (Fuchs fraction equal to one) when  $p = 1$  or  $v_z = 0$  and the lower bound when  $p = 0$  and  $|v_z| = v_F$ . The results are obtained for  $\tau^*(\mathbf{k}) = 25$  fs and  $v_F = 1.57 \cdot 10^6$  m/s, resembling a monocrystalline Cu thin film.

with:

$$\begin{aligned} \kappa &\equiv t/l_0, \\ H(\alpha, \theta, \phi) &\equiv 1 + \alpha/|\sin \theta \cos \phi|, \end{aligned} \quad (12)$$

and  $\theta$  and  $\phi$  respectively referring to the polar and azimuthal angle of the spherical coordinate system with poles located on the  $z$ -axis.

The bulk conductivity is retrieved as the limiting case

corresponding to  $R = 0$  and  $p = 1$ :

$$\begin{aligned} \sigma^{\text{bulk}} &= \sigma^{\text{GB+BS}}(\alpha = 0, p = 1) \\ &= n_e e^2 \tau / m_e = n_e e^2 l_0 / (m_e v_F). \end{aligned} \quad (13)$$

Also note that the conductivity is finite in the limit  $p \rightarrow 0$  while:

$$\begin{aligned} \lim_{\alpha \rightarrow +\infty} \sigma^{\text{GB+BS}}(\alpha, p) &= \lim_{R \rightarrow 1} \sigma^{\text{GB+BS}}(R, p) = 0, \\ \lim_{\alpha \rightarrow +\infty} \sigma^{\text{GB}}(\alpha) &= \lim_{R \rightarrow 1} \sigma^{\text{GB}}(R) = 0, \\ \lim_{p \rightarrow 1} \sigma^{\text{GB+BS}}(\alpha, p) &= \sigma^{\text{GB}}(\alpha). \end{aligned} \quad (14)$$

Analogous limiting cases can be discovered in the extended model presented in the following section.

## B. Conduction band anisotropy

We extend the Mayadas-Shatzkes model to account for an anisotropic conduction band, for which we introduce a diagonal effective mass tensor. The Fermi surface  $\epsilon(\mathbf{k}) = E_F$  is ellipsoidal and the following relations hold, while  $\mathbf{k}$  corresponds to any electron state at the Fermi level:

$$\begin{aligned} E_F &= \frac{\hbar^2 k_x^2}{2m_x} + \frac{\hbar^2 k_y^2}{2m_y} + \frac{\hbar^2 k_z^2}{2m_z} = \frac{\hbar^2 k_F^2}{2m_e}, \\ n_e &= M_x M_y M_z \frac{k_F^3}{3\pi^2} = M_x M_y M_z \frac{(2m_e E_F)^{3/2}}{3\pi^2 \hbar^3}, \\ k_F &\equiv \sqrt{2m_e E_F / \hbar}, \quad M_{x,y,z} \equiv \sqrt{m_{x,y,z} / m_e}. \end{aligned} \quad (15)$$

For Eq. (8), an isotropic magnitude of the Fermi level velocities, mean free path and collision time are considered, which needs to be modified in case of conduction band anisotropy. The electron velocity of Fermi level states is now anisotropic and given by:

$$|\mathbf{v}(\mathbf{k})| = |\nabla_{\mathbf{k}}E(\mathbf{k})/\hbar| = \hbar\sqrt{\frac{k_x^2}{m_x^2} + \frac{k_y^2}{m_y^2} + \frac{k_z^2}{m_z^2}}, \quad (16)$$

and in general this velocity magnitude can be related to an anisotropic mean free path  $l_0(\mathbf{k})$  and/or collision time  $\tau(\mathbf{k})$  through  $|\mathbf{v}(\mathbf{k})| = l_0(\mathbf{k})/\tau(\mathbf{k})$ . The grain boundary scattering probability is still given by Eq. (4), but  $R$ , the reflection coefficient of a Fermi level electron with velocity perpendicular to a grain boundary barrier, is related differently to the barrier strength due to the band anisotropy:

$$R = 1 / [1 + \hbar^4 k_F^2 / (M_x m_e S)^2]. \quad (17)$$

In order to compute the conductivity with Eq. (11), we need to integrate over an ellipsoidal Fermi surface. Hence, we define new integration variables to map it to a spherical surface integration:

$$k_{x,y,z} \rightarrow k_{x,y,z} / M_{x,y,z}. \quad (18)$$

---


$$\sigma^{\text{GB+BS}}(\beta, p) = \sigma^{\text{GB}}(\beta) - \frac{n_e e^2 \tau}{m_x} \frac{6}{\pi \lambda} (1-p) \int_0^{\pi/2} d\theta \int_0^{\pi/2} d\phi \frac{\sin^3 \theta \cos \theta \cos^2 \phi}{H^2(\beta, \theta, \phi)} \frac{1 - \exp[-\lambda H(\beta, \theta, \phi) / \cos \theta]}{1 - p \exp[-\lambda H(\beta, \theta, \phi) / \cos \theta]}, \quad (20)$$

with:

$$\begin{aligned} H(\beta, \theta, \phi) &\equiv 1 + \beta / |\sin \theta \cos \phi|, \\ \lambda &\equiv t m_z / (\hbar M_z k_F \tau) = M_z \kappa. \end{aligned} \quad (21)$$

The remaining integrations cannot be carried out analytically and are performed numerically. As a limiting case, the bulk conductivity equals

$$\sigma^{\text{bulk}} = \sigma^{\text{GB+BS}}(\beta = 0, p = 1) = n_e e^2 \tau / m_x. \quad (22)$$

## 2. Isotropic mean free path

In case of an isotropic mean free path and an ellipsoidal Fermi surface, the collision time is directional and given by

$$\tau(\mathbf{k}) = \frac{l_0 \hbar}{|\nabla_{\mathbf{k}}E(\mathbf{k})|} = \frac{l_0}{\hbar \sqrt{k_x^2/m_x^2 + k_y^2/m_y^2 + k_z^2/m_z^2}}. \quad (23)$$

Following the derivation of Mayadas and Shatzkes, the conductivity will first be calculated taking only the scattering by grain boundaries into account. Scattering at the external surfaces will be accounted for subsequently. We will consider two cases in the subsections below, the first one assuming an isotropic collision time, the second one an isotropic mean free path. The former is relevant for electron-phonon interactions while the latter is more suitable for the low temperature regime dominated by impurity and defect scattering.

### 1. Isotropic collision time

Using the result of Eq. (17) and the rescaling according to Eq. (18), we solve for the conductivity, given by Eq. (7), for an ellipsoidal Fermi surface with isotropic collision time  $\tau$ :

$$\begin{aligned} \sigma^{\text{GB}}(\beta) &= \frac{n_e e^2 \tau}{m_x} 3 \left[ \frac{1}{3} - \frac{\beta}{2} + \beta^2 - \beta^3 \ln \left( \frac{1+\beta}{\beta} \right) \right], \\ \beta &\equiv 2\tau \frac{\hbar k_F}{M_x m_e d} \frac{R}{1-R} = \frac{\alpha}{M_x}. \end{aligned} \quad (19)$$

In order to include scattering at the film boundary surfaces we adopt the Fuchs-Sondheimer approach as before:

---

The conductivity expression for grain boundary scattering cannot be obtained analytically in this case and is given by:

$$\sigma^{\text{GB}}(\alpha) = \frac{n_e e^2 \tau_x}{m_x} \frac{6}{\pi} \int_0^{\pi/2} d\theta \int_0^{\pi/2} d\phi \frac{\sin^3 \theta \cos^2 \phi}{\zeta(\theta, \phi) + \alpha / |\sin \theta \cos \phi|}, \quad (24)$$

where  $\tau_x \equiv l_0 m_x / (\hbar M_x k_F)$  and

$$\zeta(\theta, \phi) \equiv \sqrt{\sin^2 \theta \cos^2 \phi + \sin^2 \theta \sin^2 \phi \frac{M_x^2}{M_y^2} + \cos^2 \theta \frac{M_x^2}{M_z^2}}. \quad (25)$$

The extension for scattering at the film boundary surfaces is again obtained in a straightforward manner:

$$\sigma^{\text{GB+BS}}(\alpha, p) = \sigma^{\text{GB}}(\alpha) - \frac{n_e e^2 \tau_x}{m_x} \frac{6}{\pi \mu} (1-p) \int_0^{\pi/2} d\theta \int_0^{\pi/2} d\phi \frac{\sin^3 \theta \cos \theta \cos^2 \phi}{G^2(\alpha, \theta, \phi)} \frac{1 - \exp[-\mu G(\alpha, \theta, \phi)/\cos \theta]}{1 - p \exp[-\mu G(\alpha, \theta, \phi)/\cos \theta]}, \quad (26)$$

with:

$$G(\alpha, \theta, \phi) \equiv \zeta(\theta, \phi) + \alpha/|\sin \theta \cos \phi|, \quad (27)$$

$$\mu \equiv M_z t / (M_x l_0) = \lambda / M_x = M_z \kappa / M_x.$$

The bulk limit ( $\alpha = 0, p = 1$ ) also requires numerical integration in this case, with  $1/\zeta(\theta, \phi)$  in the integrand.

### C. Directional effective mass fit

The aim of the fitting procedure in this subsection is to obtain an anisotropic effective mass model with an ellipsoidal energy-momentum relation that captures the anisotropic bulk conductivity of an arbitrary Fermi surface in the best possible way, thereby providing appropriate directional effective mass values for the semiclassical resistivity scaling model. The computational procedure for extracting the conductivity is presented below for a particular transport direction ( $x$ ) and without imposing any Fermi surface averaging (as might be appropriate for monocrystalline thin films). Nevertheless, it can be generalized to an arbitrary transport direction with any type of averaging (e.g. in-plane or isotropic averaging) in a straightforward manner (see Appendix B).

We start from the bulk conductivity expression for an arbitrary Fermi surface as obtained from Eq. (3), without grain boundary scattering term, and with an additional conduction band label  $n$ :

$$\sigma_x^{\text{bulk}} = -\frac{e^2}{4\pi^3} \sum_n \int d^3v \frac{v_x^2 n(\mathbf{v}) \tau_n(\mathbf{v})}{|\partial \mathbf{v} / \partial \mathbf{k}|} \frac{\partial f_n^{\text{eq}}(\epsilon(\mathbf{v}))}{\partial \epsilon} \quad (28)$$

$$\approx \frac{e^2}{4\pi^3} \int d^2\Omega g_x(\theta, \phi),$$

where an integration over the surface of the unit sphere in the last line is obtained by introducing the following approximation for the derivative of the Fermi-Dirac distribution function at low temperatures ( $k_B T \ll E_F$ ) by:

$$\frac{\partial f_n^{\text{eq}}(\epsilon(\mathbf{k}))}{\partial \epsilon} \approx -\frac{\vartheta[2\delta E - |\epsilon_n(\mathbf{k}) - E_F|]}{4\delta E}, \quad (29)$$

with  $\vartheta(\epsilon)$  the Heaviside step function,  $\delta E > 0$  very small and the following definition of  $g_x(\theta, \phi)$ :

$$g_x(\theta, \phi) \equiv \int_0^{+\infty} dv v^2 \sum_n \frac{v_x^2 n(\mathbf{v}) \tau_n(\mathbf{v})}{\det |\partial \mathbf{v}(\mathbf{k}) / \partial \mathbf{k}|} \quad (30)$$

$$\times \frac{\vartheta[2\delta E - |\epsilon_n(\mathbf{v}) - E_F|]}{4\delta E}.$$

The integration is carried out over group velocities instead of wave vectors as the directionality of the former is more physically relevant, underlying the semiclassical boundary conditions for partial specular surface scattering in Eq. (10). The bulk conductivity in Eq. (28) will be approximated by considering the Fermi surface of a single conduction band with ellipsoidal energy-momentum relation as introduced in Eq. (15), which can be rewritten in terms of Fermi velocities  $\mathbf{v}$  as:

$$a_x v_x^2 + a_y v_y^2 + a_z v_z^2 = 1, \quad a_{x,y,z} \equiv M_{x,y,z}^2 m_e / (2E_F), \quad (31)$$

such that we get a bulk conductivity:

$$\sigma_x^{\text{bulk}} \approx \frac{e^2}{4\pi^3} \int d^2\Omega h_x(\theta, \phi), \quad (32)$$

$$h_x(\theta, \phi) \equiv \frac{4E_F^2}{\hbar^3} a_x a_y a_z \sin^2 \theta \cos^2 \phi v_F^5(\theta, \phi) \tau(\theta, \phi).$$

We would like to fix  $a_x$ ,  $a_y$ ,  $a_z$  and  $E_F$  such that  $g_x(\theta, \phi) \approx h_x(\theta, \phi)$  for all angles  $\theta$  and  $\phi$ , properly reflecting the bulk conductivity contributions of electron states with a differently oriented velocity. Note that this fitting procedure does not involve any matching of quantities involving electron states away from the Fermi level, such as the work function of the metal or the band curvature of the bottom of a conduction band emerging from the *ab initio* band structure. Furthermore, the fit in velocity space does not capture the full distribution of electron states in the Brillouin zone (e.g. centered around different symmetry points), as can be expected when adopting the effective mass approximation. A suitable fit can be obtained by combining  $g_x(\theta, \phi) \approx h_x(\theta, \phi)$  and Eq. (31) to obtain a system of equations which can be solved with the least-squares method. The resulting system of equations will depend on the functional form adopted for  $\tau(\theta, \phi)$ . In case of an isotropic bulk collision time, we obtain:

$$\begin{aligned} \forall \theta, \phi: \quad \tau(\theta, \phi) = \tau, \quad v_F^2(\theta, \phi) &\approx [\hbar^3 g_x(\theta, \phi) / (4E_F^2 a_x a_y a_z \sin^2 \theta \cos^2 \phi \tau)]^{2/5}, \\ \Rightarrow \frac{a_x \sin^2 \theta \cos^2 \phi}{(E_F^2 a_x a_y a_z)^{2/5}} + \frac{a_y \sin^2 \theta \sin^2 \phi}{(E_F^2 a_x a_y a_z)^{2/5}} + \frac{a_z \cos^2 \theta}{(E_F^2 a_x a_y a_z)^{2/5}} &= \left( \frac{4 \sin^2 \theta \cos^2 \phi \tau}{\hbar^3 g_x(\theta, \phi)} \right)^{2/5}, \end{aligned} \quad (33)$$

where the right-hand side is independent of the fitting parameters and the left-hand side contains three inde-

pendent parameters. In case of an isotropic mean free path  $l_0$ , we get in a completely analogous way:

$$\begin{aligned} \forall \theta, \phi: \quad \tau(\theta, \phi) = l_0 / v_F(\theta, \phi), \quad v_F^2(\theta, \phi) &\approx [\hbar^3 g(\theta, \phi) / (4E_F^2 a_x a_y a_z \sin^2 \theta \cos^2 \phi l_0)]^{1/2} \\ \Rightarrow \frac{a_x \sin^2 \theta \cos^2 \phi}{E_F (a_x a_y a_z)^{1/2}} + \frac{a_y \sin^2 \theta \sin^2 \phi}{E_F (a_x a_y a_z)^{1/2}} + \frac{a_z \cos^2 \theta}{E_F (a_x a_y a_z)^{1/2}} &= \left( \frac{4 \sin^2 \theta \cos^2 \phi l_0}{\hbar^3 g_x(\theta, \phi)} \right)^{1/2}. \end{aligned} \quad (34)$$

Some freedom remains in the choice of  $a_x$ ,  $a_y$ ,  $a_z$  and  $E_F$ . The fitting parameters allow for the Fermi energy and effective masses to scale as  $E_F \rightarrow CE_F$ ,  $M_{x,y,z} \rightarrow C^{-3/2} M_{x,y,z}$  when the collision time is isotropic, and as  $E_F \rightarrow CE_F$ ,  $M_{x,y,z} \rightarrow C^{-1/2} M_{x,y,z}$  when the mean free path is isotropic. This remaining degree of freedom can be eliminated by matching the density of states at the Fermi level of the anisotropic effective mass model and of the *ab initio* band structure:

$$\begin{aligned} \frac{dn_e}{dE_F} &= (a_x a_y a_z)^{1/2} \frac{4E_F^2}{\pi^2 \hbar^3} \\ &= 2 \int \frac{d^3 k}{(2\pi)^3} \sum_n \frac{\vartheta[2\delta E - |\epsilon_n(\mathbf{k}) - E_F|]}{4\delta E}. \end{aligned} \quad (35)$$

The Fermi level density of states of the anisotropic effective mass remains constant under rescaling  $E_F \rightarrow CE_F$ ,  $M_{x,y,z} \rightarrow C^{-1/6} M_{x,y,z}$ , which is different from the invariance of the conductivity in the case of an isotropic collision time or mean free path.

### III. RESULTS

The metal thin film conductivity (or resistivity) scaling formulas, derived under the assumption of an isotropic collision time (Eq. 20) and an isotropic mean free path (Eq. 26), are evaluated for different parameters and degrees of conduction band anisotropy in Fig. 2, fixing the reflection coefficient and specularity parameter to the same value of 0.5 and the average linear intercept equal to the film thickness ( $d = t$ ). The following effective masses are considered:  $M_x = M_y = M$  and  $M_z = 1/M^2$ , with eccentricity parameter  $M > 0$ . This represents an ellipsoidal (prolate when  $M < 1$  and oblate when  $M > 1$ ) conduction band with in-plane ( $x$ - $y$ ) versus out-of-plane ( $z$ ) anisotropy. Furthermore, the anisotropy is tuned by  $M$  without changing the density of states at the Fermi level, which can be understood from Eq. 15. All resistivity scaling curves show similar behavior with

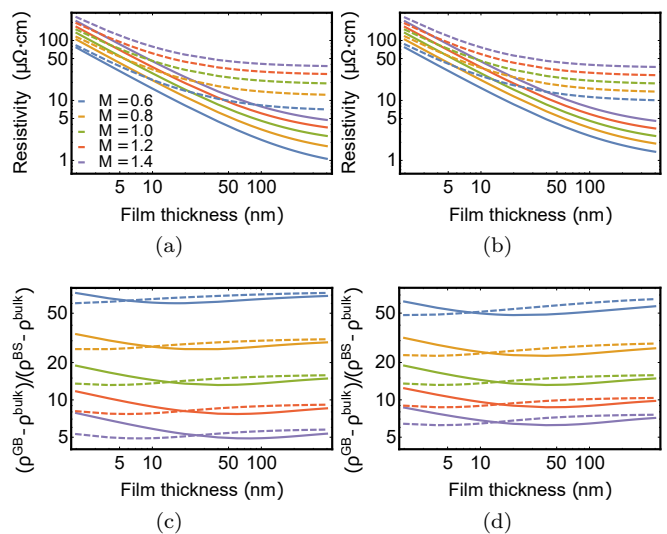


FIG. 2. (a-b) The resistivity is evaluated as a function of the film thickness, considering a Fermi energy of 5 eV, reflection coefficient  $R = 0.5$  and specularity parameter  $p = 0.5$  for different degrees of out-of-plane anisotropy by varying the eccentricity parameter  $M$  ( $M_x = M_y = M$ ,  $M_z = 1/M^2$ ), assuming (a) an isotropic collision time of 37.7 fs (full lines) and 3.77 fs (dashed lines) (b) an isotropic mean free path of 50 nm (full lines) and 5 nm (dashed lines). The values of collision time and mean free path are equivalent choices when  $M = 1$ . (c-d) The ratio of the resistivity contributions due to grain boundary and boundary surface scattering is evaluated as a function of the film thickness, considering either an isotropic collision time (c), or an isotropic mean free path (d).

lower in-plane mass and higher out-of-plane mass resulting in a lower resistivity for all film thicknesses. The bulk collision time or mean free path predominantly affects the large film thickness behavior which is found to approach the bulk resistivity limit. The resistivity is dominated by grain boundary backscattering for all degrees of anisotropy, increasingly for lower (higher) in-

		Isotropic				
Texture	quantity	$M_x$	$M_y$	$M_z$	$E_F$ (eV)	
Cu	any	$\tau$	1.23	1.23	1.23	4.52
		$l_0$	1.25	1.25	1.25	3.93
Ru	[001]	$\tau$	1.65	1.65	1.54	5.00
		$l_0$	1.91	1.91	1.62	2.54
	none	$\tau$	1.69	1.69	1.69	3.71
		$l_0$	1.72	1.72	1.72	3.37

TABLE I. Least square fit of the diagonal effective mass tensor and Fermi energy for bulk Cu and Ru following the procedure of section II C with Eqs. (33)-(34).

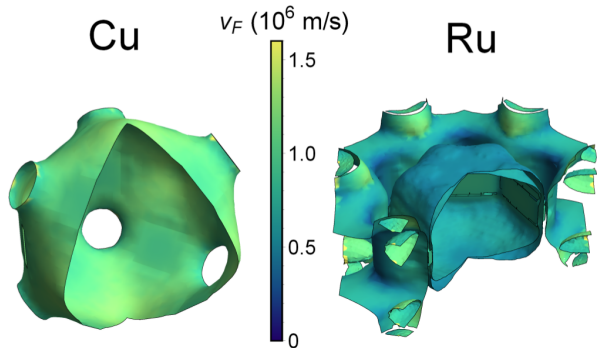


FIG. 3. The Fermi surface is shown for bulk Cu and Ru with the magnitude of the directional Fermi velocity indicated in color.

plane (out-of-plane) effective masses. The ratio of resistivity due to grain boundary versus boundary surface scattering reaches a minimum when the film thickness is of the order of the bulk mean free path, the minimum shifting up for a higher (lower) in-plane (out-of-plane) effective mass.

According to the fitting procedure of section II C (see Appendix B for more details), the directional effective masses and Fermi energy were obtained for bulk Cu and Ru, as presented in Table I. For Ru, we consider untextured films for which a spherically averaged Fermi surface with  $M_x = M_y = M_z$  is appropriate, as well as [001]-textured films for which in-plane ( $x$ - $y$ ) averaging ( $M_x = M_y \neq M_z$ ) of the Fermi surface is appropriate. All the subsequent results depend on the film texture under consideration. For Cu the Fermi surface is quasi-isotropic, hence the fit does not depend on the film texture. The bulk Fermi surfaces for Cu and Ru (see Fig. 3) were obtained with the computation of the bulk electronic structures using *ab initio* calculations based on the density functional theory implemented in the Quantum-Espresso packages [31]. Projector augmented wave [32] potentials with the Perdew-Burke-Ernzerof generalized gradient [33] approximation form of the exchange-correlation functional and a finer Monkhorst-Pack  $k$ -point sampling grid of 40x40x40 together with kinetic energy cutoff of 80 Ry are used to

Texture	$\rho_{x-y}$ ( $\mu\Omega\cdot\text{cm}$ )	$\rho_z$ ( $\mu\Omega\cdot\text{cm}$ )	$\tau$ (fs)	$l_0$ (nm)
Cu	any	1.71	1.71	38.8
Ru	none	7.05	7.05	9.2
	[001]	7.62	5.82	6.0

TABLE II. Values for the (isotropic) collision time ( $\tau$ ) and mean free path ( $l_0$ ) are listed for Cu and untextured and [001]-textured Ru films, as obtained from the fitted effective masses and Fermi energy in Table I, the bulk limit of Eqs. (20) and (26), and the experimental resistivity values at 300 K (in-plane:  $\rho_{x-y}$ , out-of-plane:  $\rho_z$ ) [34].

ensure the total energy to converge up to a tolerance of 10-12 eV.

Based on the fit for the effective masses and the Fermi energy, the value of  $\sigma^{\text{bulk}}/\tau$  or  $\sigma^{\text{bulk}}/l_0$  can be obtained, assuming an isotropic bulk collision time or an isotropic bulk mean free path, by plugging the obtained values into the bulk limit of Eqs. (20) and (26) respectively. We extract a value for the isotropic collision time or mean free path by fixing the resistivity along the transport direction to the experimental value at room temperature [34]. The obtained values are provided in Table II.

We have now fixed all the parameters that enter the conductivity formulas in Eqs. (20) and (26), based on *ab initio* Fermi surface calculations and calibration with bulk resistivity data, apart from the reflection coefficient  $R$ , the specularly parameter  $p$  and the average linear intercept  $d$  between grains. The average linear intercept can be estimated from TEM images of the thin film samples, such that the reflection coefficient  $R$  and specularly parameter  $p$  are the two remaining fitting parameters. We will fit  $R$  and  $p$  to experimental thickness-dependent resistivity and intercept data of to both Cu and Ru films. Cu films were deposited by physical-vapor deposition (PVD, sputtering) at room temperature on 1.5 nm TaN/SiO<sub>2</sub>/Si substrates and capped by 1.5 nm of TaN to prevent oxidation of Cu. The films showed an fcc crystalline structure with strong [111] texture [21]. PVD Ru films were deposited on SiO<sub>2</sub>/Si substrates, leading to strong hexagonal [001] texture [21]. Additional Ru films were deposited by atomic layer deposition on TiN/SiO<sub>2</sub>/Si substrates leading to the absence of any texture in the films, i.e. the films were random hexagonal polycrystals [35]. Thin film resistivities were obtained from four-point sheet resistance measurements at room temperature as well as the film thickness measured by both x-ray reflectance and Rutherford backscattering spectrometry [21].

As the relation  $d(t)$  is required for all thicknesses  $t$  and only available for certain sample thicknesses, linear interpolation was used with the addition of a virtual data point ( $t = 0, d = 0$ ) (appropriate for very thin imperfect films). All the fitted parameters for the different sets of data and different assumptions for film texture and bulk scattering (isotropic collision time or isotropic mean free path) are listed in Table III and the resulting resistivity

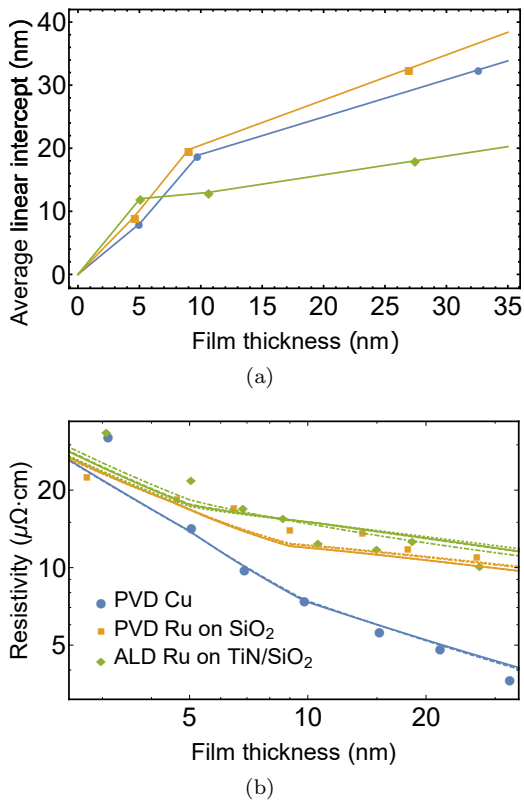


FIG. 4. (a) Experimental values for the average linear intercept as a function of the film thickness. Piecewise linear interpolation is considered for the resistivity scaling model. (b) Resistivity scaling fits and experimental resistivity data on a log-log scale of PVD Cu, PVD Ru on  $\text{SiO}_2$  and ALD Ru on  $\text{TiN/SiO}_2$ . The fits for  $p$  and  $R$  are listed in Table III. They are obtained for Cu and untextured Ru, assuming isotropic  $\tau$  (full) or isotropic  $l_0$  (dashed), as well as for [001]-textured Ru with isotropic  $\tau$  (dotted) or isotropic  $l_0$  (dot-dashed).

curves are shown in Fig. 4 (b). The steep resistivity increase for PVD Cu and PVD Ru below a film thickness of 7 nm could not be fitted satisfactorily with any set of parameters  $R$  and  $p$ . Therefore, the presented fits for the PVD data have been obtained without considering the data point for thickness around 3 nm (still under-shooting the PVD Ru data point around 5 nm thickness systematically). Even though different film textures and bulk scattering properties underlie the different resistivity scaling curves of a given data set, the curves are in very close agreement.

The SSE of the full range of  $R$  and  $p$  is shown for all the combinations of film texture and bulk scattering assumptions for the different fits in Figs. 5-6, with the results of Table III indicated. The fit is very robust for the reflection coefficient  $R$ , unlike for the specularity parameter  $p$ . Furthermore, slight differences between the reflection coefficients can be identified when considering a [001]-textured thin film with isotropic collision time or mean free path for PVD and ALD Ru. Assuming an isotropic collision time (mean free path), increases (decreases) the

		Isotropic			
	Texture	quantity	$R$	$p$	$\sqrt{\text{SSE}}$ ( $\mu\Omega\cdot\text{cm}$ )
PVD Cu	<u>any</u>	$\tau$	<u>0.22</u>	<u>0.02</u>	<u>0.86</u>
		$l_0$	0.18	0.00	0.86
PVD Ru	none	$\tau$	0.45	0.99	4.72
		$l_0$	0.43	0.94	4.71
	<u>[001]</u>	$\tau$	<u>0.48</u>	<u>0.96</u>	<u>4.08</u>
		$l_0$	0.37	1.00	4.25
ALD Ru	none	$\tau$	<u>0.40</u>	<u>0.00</u>	<u>5.94</u>
		$l_0$	0.38	0.00	5.80
	<u>[001]</u>	$\tau$	0.43	0.00	6.28
		$l_0$	0.26	0.00	4.80

TABLE III. Values for the reflection coefficient  $R$  and specularity parameter  $p$  for the different metal thin films under consideration with the different assumptions for the electronic structure and dominant bulk scattering process. The appropriate set of assumptions for each set of data is underlined.

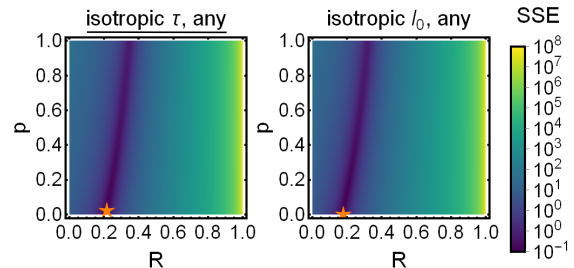


FIG. 5. The SSE of the fit of (a) Eq. (20) (b) Eq. (26) to the PVD Cu data of Fig. 4 is shown for  $0 \leq R, p \leq 1$ . The minimum is indicated with a star.

obtained reflection coefficient with respect to the untextured film assumption, for which the assumption regarding the bulk scattering isotropy is of little importance. The specularity parameter is in general barely affected.

#### IV. DISCUSSION

It is clear from the results that conduction band anisotropy can have an impact on thin film resistivity scaling. The resistivity curves with different degrees of in-plane versus out-of-plane anisotropy in Fig. 2 clearly show the impact on resistivity scaling, the lowest resistivity being realized by the lowest in-plane and highest out-of-plane effective masses. As such, the electrons suffer less from boundary scattering and are more resilient to grain boundary scattering. The impact is more pronounced in case of an isotropic collision time as compared to an isotropic mean free path and this can be understood by having a closer look at the conductivity expressions in Eqs. (11), (20) and (26). In case of an isotropic collision time, both the effective mass along the transport direction and the parameter for grain boundary scattering

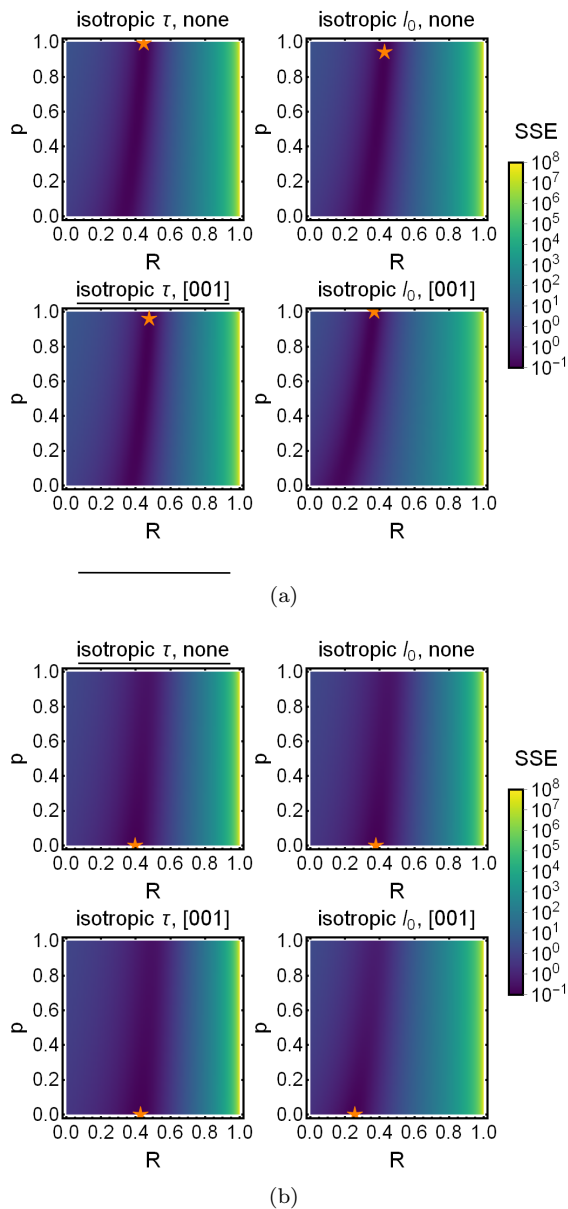


FIG. 6. The SSE of the fit of Eqs. (20) for isotropic collision time (left column) and (26) for isotropic mean free path (right column) to the (a) PVD Ru on  $\text{SiO}_2$  (b) ALD Ru on  $\text{TiN/SiO}_2$  data of Fig. 4 is shown for  $0 \leq R, p \leq 1$ , assuming an untextured (top row) and a [001]-textured film (bottom row). The minimum is indicated with a star.

are renormalized w.r.t. the Mayadas-Shatzkes formula ( $m_e \rightarrow m_x$ ,  $\alpha \rightarrow \beta$ ). As the latter is not renormalized in case of an isotropic mean free path, the impact of anisotropy is more limited.

When the average linear intercept is comparable to the film thickness, grain boundary scattering is typically more detrimental to the conductivity than boundary surface scattering. This feature can clearly be seen in Fig. 2 and has also been observed before [21, 36]. The reason for this is that backscattering at grain boundaries is

maximally detrimental to the electron transport velocity, which gets completely reversed by the scattering event ( $v_x \rightarrow -v_x$ ). Conversely, a diffusive boundary scattering event reorients the velocity arbitrarily, possibly retaining or even enhancing the transport velocity of a conduction electron. This property is also reflected in the robustness of the reflection coefficient  $R$  in all the fits, while the obtained value for  $p$  can easily swing up or down for minor variations in the data or for different assumptions regarding the film texture and bulk scattering properties. One should therefore be careful drawing any conclusion from the precise value of  $p$  in these fits, as it carries little physical significance.

While the quality of the fit to thickness-dependent resistivity data and the value of the specularly parameter barely depend on the different assumptions for film texture and bulk scattering (isotropy of bulk collision time or mean free path), the obtained value of the grain boundary reflection coefficient can be affected. When attempting to draw meaningful conclusions on grain boundary scattering from the precise value of the reflection coefficient, one should also consider the film texture and degree of conduction band anisotropy as well as the characteristics of the dominant bulk scattering mechanism before proceeding with the appropriate fitting procedure. These complications arise only when one considers metals with a high degree of anisotropy, such that one has to go beyond the standard Mayadas-Shatzkes formula. For Cu, the conduction band is nearly isotropic and the different assumptions lead to results that are in close agreement.

All the resistivity measurements in the fits were performed at room temperature, so we expect the (acoustic) phonons to provide the dominant scattering mechanism in the bulk regime, rendering the isotropic collision time assumption and the corresponding  $R$  parameters meaningful. Furthermore, the [001]-textured film assumption should apply to PVD Ru while the results with a untextured film assumption should be considered for ALD Ru, even though this does not provide the best overall fit. The appropriateness of the fit is not reflected in the quality of the fit, but it certainly dismisses the validity of certain results under different assumptions. For example, the reflection coefficient would turn out to be significantly larger for the Ru samples if the [001]-texture with isotropic bulk mean free path would be the appropriate assumption.

A returning problem of the Mayadas-Shatzkes model and its extension for anisotropic conduction bands is the underestimation of the resistivity for small film thicknesses (for PVD Cu and PVD Ru on  $\text{SiO}_2$  in our case) [37]. While it is hard to guarantee film continuity for the samples at very low thicknesses, several limitations and approximations underlying the Mayadas-Shatzkes model and its extension (including the consideration of a three-dimensional wave vector, the phenomenological treatment of boundary surface scattering and the perturbative treatment of grain boundary scattering) could also be (partially) responsible for a systematic underestima-

tion (already remarked by Choi *et al.* [22]). A recent validity analysis by Moors *et al.* showed that this is certainly the case for a perturbative treatment of boundary surface scattering due to surface roughness and grain boundary scattering for extremely narrow nanowires [11]. Additionally, the consideration of a (diagonal) effective mass (tensor) could be too approximate for complicated Fermi surfaces. A full numerical simulation of Eq. 9 with the correct Fermi surface for different thicknesses should be able to rule this out.

In recent work, Li *et al.* introduced a phenomenological correction for conduction band anisotropy and argued that it was responsible for the sharper resistivity increase at small thicknesses for Os films [26]. Our results do not agree with this as they cannot explain an underestimation of the resistivity for small thicknesses merely based on conduction band anisotropy. Another issue that might explain the deviations is the lack of data on average linear intercepts below 5 nm thickness. Since grain boundary scattering is dominant, the resistivity curve will be strongly dependent on the value of  $d$ , hence an accurately determined value of the average linear intercept is crucial for the fitting procedure. The linear interpolation that we employed might be too limited.

## V. CONCLUSION

The semiclassical resistivity scaling formula derived by Mayadas and Shatzkes for metal thin films with grain boundary and boundary surface scattering is extended to account for conduction band anisotropy. Apart from a dependency on the film texture, this extension introduces an additional dependency on the anisotropy of the

dominant bulk scattering mechanism. An explicit formulation for the thickness-dependent resistivity is derived and presented for two limit cases: bulk scattering with an isotropic collision time and with an isotropic mean free path.

A systematic procedure is presented to fit a (or multiple) highly anisotropic conduction band(s) of a metal of choice to an ellipsoidal Fermi surface and then demonstrated for Cu and Ru, respectively nearly isotropic and highly anisotropic. This procedure allows us to systematically fit the grain boundary reflection coefficient and specularity parameter of the film boundary surfaces for textured and untextured metal thin films with anisotropic conduction bands. A dependency of the reflection coefficient on the film texture and the bulk scattering characteristics is observed, while the obtained specularity parameter is barely unaffected and moreover physically insignificant due to the resistivity contribution of boundary surface scattering being much weaker. While conduction band anisotropy has been suggested before as a possible explanation for deviations from Mayadas-Shatzkes (e.g. a steeper resistivity increase for very small film thicknesses), this hypothesis does not follow from our model. The main consequence of considering conduction band anisotropy is a renormalization of the reflection coefficient, without significantly adjusting the quality of the fit to experimental thickness-dependent resistivity data.

## ACKNOWLEDGMENTS

The authors acknowledge the support by the National Research Fund Luxembourg (ATTRACT Grant No. 7556175).

- 
- [1] K. Fuchs, Proceedings of Cambridge Philosophical Society **34**, 100 (1938).
  - [2] E. H. Sondheimer, Advances in Physics **1**, 1 (1952).
  - [3] A. Mayadas and M. Shatzkes, Physical Review B **1**, 1382 (1970).
  - [4] S. B. Soffer, Journal of Applied Physics **38**, 1710 (1967).
  - [5] N. Trivedi and N. W. Ashcroft, Physical Review B **38**, 12298 (1988).
  - [6] G. Fishman and D. Calecki, Physical Review Letters **62**, 1302 (1989).
  - [7] X.-G. Zhang and W. H. Butler, Physical Review B **51**, 10085 (1995).
  - [8] G. Palasantzas, Physical Review B **58**, 9685 (1998).
  - [9] A. E. Meyerovich and I. V. Ponomarev, Physical Review B **65**, 155413 (2002).
  - [10] J. M. Rickman and K. Barmak, Journal of Applied Physics **112**, 013704 (2012).
  - [11] K. Moors, B. Sorée, and W. Magnus, Journal of Physics Condensed Matter **28**, 1 (2016).
  - [12] R. C. Munoz and C. Arenas, Applied Physics Reviews **4**, 011102 (2017).
  - [13] J. W. C. De Vries, Thin Solid Films **167**, 25 (1988).
  - [14] H.-D. Liu, Y.-P. Zhao, G. Ramanath, S. P. Murarka, and G.-C. Wang, Thin Solid Films **384**, 151 (2001).
  - [15] M. Tay, K. Li, and Y. Wu, Journal of Vacuum Science & Technology B **23**, 1412 (2005).
  - [16] J. M. Camacho and A. Oliva, Thin Solid Films **515**, 1881 (2006).
  - [17] T. Sun, B. Yao, A. P. Warren, K. Barmak, M. F. Toney, R. E. Peale, and K. R. Coffey, Physical Review B **81**, 155454 (2010).
  - [18] J. S. Chawla, F. Gstrein, K. P. O'Brien, J. S. Clarke, and D. Gall, Physical Review B **84**, 235423 (2011).
  - [19] K. Sankaran, S. Clima, M. Mees, and G. Pourtois, ECS Journal of Solid State Science and Technology **4**, N3127 (2015).
  - [20] D. Gall, Journal of Applied Physics **119**, 085101 (2016).
  - [21] S. Dutta, K. Sankaran, K. Moors, G. Pourtois, S. Van Elshocht, J. Bömmels, W. Vandervorst, Z. Tókei, and C. Adelmann, Journal of Applied Physics **122** (2017).
  - [22] D. Choi, X. Liu, P. K. Schelling, K. R. Coffey, and K. Barmak, Journal of Applied Physics **115**, 104308 (2014).
  - [23] S. L. Jones, A. Sanchez-Soares, J. J. Plombon, A. P.

- Kaushik, R. E. Nagle, J. S. Clarke, and J. C. Greer, *Physical Review B* **92**, 115413 (2015).
- [24] G. Hegde, R. C. Bowen, and M. S. Rodder, *Applied Physics Letters* **109**, 193106 (2016).
- [25] N. A. Lanzillo, *Journal of Applied Physics* **121**, 175104 (2017).
- [26] S. L. Li, Q. Y. Zhang, C. Y. Ma, C. Zhang, Z. Yi, and L. J. Pan, *Journal of Applied Physics* **121**, 134503 (2017).
- [27] A. Standard, West Conshocken (1996).
- [28] C. Jacoboni, *Theory of Electron Transport in Semiconductors: A Pathway from Elementary Physics to Nonequilibrium Green Functions*, Vol. 165 (Springer Science & Business Media, 2010).
- [29] G. D. Mahan, *Many-particle physics* (Springer Science & Business Media, 2013).
- [30] K. Moors, B. Sorée, and W. Magnus, *Microelectronic Engineering* **167**, 37 (2017).
- [31] P. Giannozzi, S. Baroni, N. Bonini, M. Calandra, R. Car, C. Cavazzoni, D. Ceresoli, G. L. Chiarotti, M. Cococcioni, I. Dabo, A. Dal Corso, S. de Gironcoli, S. Fabris, G. Fratesi, R. Gebauer, U. Gerstmann, C. Gougoussis, A. Kokalj, M. Lazzeri, L. Martin-Samos, N. Marzari, F. Mauri, R. Mazzarello, S. Paolini, A. Pasquarello, L. Paulatto, C. Sbraccia, S. Scandolo, G. Sclauzero, A. P. Seitsonen, A. Smogunov, P. Umari, and R. M. Wentzcovitch, *Journal of Physics: Condensed Matter* **21**, 395502 (2009).
- [32] P. E. Blöchl, *Physical Review B* **50**, 17953 (1994).
- [33] J. P. Perdew, K. Burke, and M. Ernzerhof, *Physical Review Letters* **77**, 3865 (1996).
- [34] J. Bass, J. Dugdale, C. Foiles, and A. Myers, *Metals: Electronic Transport Phenomena: Electrical Resistivity, Thermoelectrical Power and Optical Properties*, Vol. Landolt-Börnstein III 15B (Springer-Verlag Berlin Heidelberg, 1985).
- [35] M. Popovici, B. Groven, K. Marcoen, Q. M. Phung, S. Dutta, J. Swerts, J. Meersschant, J. A. van den Berg, A. Franquet, A. Moussa, K. Vanstreels, P. Lagrain, H. Bender, M. Jurczak, S. Van Elshocht, A. Delabie, and C. Adelman, *Chemistry of Materials* **29**, 4654 (2017).
- [36] T. Sun, B. Yao, A. P. Warren, K. Barmak, M. F. Toney, R. E. Peale, and K. R. Coffey, *Physical Review B* **79**, 041402 (2009).
- [37] P. Y. Zheng, T. Zhou, B. J. Engler, J. S. Chawla, R. Hull, and D. Gall, *Journal of Applied Physics* **122**, 095304 (2017).

### Appendix A: Transition probability for grain boundary scattering

Fermi's golden rule prescribes a transition probability  $P(\mathbf{k}, \mathbf{k}')$  from an initial state  $|i\rangle$  with wave vector  $\mathbf{k}$  to a final state  $|f\rangle$  with wave vector  $\mathbf{k}'$ :

$$P(\mathbf{k}, \mathbf{k}') = \frac{2\pi}{\hbar} |\langle f | V | i \rangle|^2 \delta(E_i - E_f). \quad (\text{A1})$$

The squared matrix element for the Mayadas-Shatzkes grain boundary potential yields:

$$\begin{aligned} & |\langle f | V^{\text{GB}} | i \rangle|^2 \\ &= \delta_{\mathbf{k}_\perp, \mathbf{k}'_\perp} \left( \frac{S}{L} \right)^2 \sum_{n, n'} \exp [i(k_x - k'_x)(x_n - x_{n'})], \end{aligned} \quad (\text{A2})$$

with  $n$  and  $n'$  ranging from 1 to  $N$ . As a result we obtain

$$\begin{aligned} P(\mathbf{k}, \mathbf{k}') &= \frac{m_x S^2}{\hbar^3 L |k_x|} \delta_{\mathbf{k}_\perp, \mathbf{k}'_\perp} \delta_{k_x, -k'_x} \\ &\times \sum_{n, n'} \exp [i(k_x - k'_x)(x_n - x_{n'})], \end{aligned} \quad (\text{A3})$$

where we rewrote the Dirac delta function as  $\delta(E_i - E_f) = m_x L / (2\pi \hbar^2 |k'_x|) \delta_{k_x, -k'_x}$ . The average of Eq. (A3) with the Gaussian distribution function of Eq. (2) yields the result of Eq. (4), with  $m_x = m_e$ .

### Appendix B: Effective mass fits for textured and untextured thin films

In order to fit a diagonal effective mass tensor to a Fermi surface as presented in Fig. 3 while properly reflecting the symmetries of a textured or untextured polycrystalline thin film with differently oriented grains, an averaging procedure is introduced. We take the appropriate average over all possible orientations of the Fermi surface that can occur in the different grains. For untextured thin films, the values of  $g(\theta, \phi)$  that are obtained from the *ab initio* data should be replaced with values that are averaged over all angles:

$$\begin{aligned} g_x(\theta, \phi) &\rightarrow \tilde{g}_x(\theta, \phi) = \sin^2 \theta \cos^2 \phi \\ &\times \frac{1}{4\pi} \int_0^\pi d\tilde{\theta} \sin \tilde{\theta} \int_0^{2\pi} d\tilde{\phi} \int_0^{+\infty} dv v^2 \\ &\times \sum_n \frac{v_n^2(\tilde{\mathbf{v}}) \tau_n(\tilde{\mathbf{v}})}{\det |\partial \tilde{\mathbf{v}}(\mathbf{k}) / \partial \mathbf{k}|} \frac{\vartheta [2\delta E - |\epsilon_n(\tilde{\mathbf{v}}) - E_F|]}{4 \delta E}, \end{aligned} \quad (\text{B1})$$

where  $\tilde{\mathbf{v}} \equiv (v, \tilde{\theta}, \tilde{\phi})$  in polar coordinates. For [001]-textured (along  $z$ ) films, the Fermi surface should be averaged over all directions in the  $x$ - $y$  plane, requiring the following replacement:

$$\begin{aligned} g_x(\theta, \phi) &\rightarrow \tilde{\tilde{g}}_x(\theta, \phi) = \sin^2 \theta \cos^2 \phi \frac{1}{2\pi} \int_0^{2\pi} d\tilde{\phi} \int_0^{+\infty} dv v^2 \\ &\times \sum_n \frac{v_n^2(\tilde{\tilde{\mathbf{v}}}) \tau_n(\tilde{\tilde{\mathbf{v}}})}{\det |\partial \tilde{\tilde{\mathbf{v}}}(\mathbf{k}) / \partial \mathbf{k}|} \frac{\vartheta [2\delta E - |\epsilon_n(\tilde{\tilde{\mathbf{v}}}) - E_F|]}{4 \delta E}, \end{aligned} \quad (\text{B2})$$

where  $\tilde{\tilde{\mathbf{v}}} \equiv (v, \theta, \tilde{\phi})$  in polar coordinates.

The least-squares fits of Eq. (33) and Eq. (34) presented in Table I were obtained with 500 pairs of  $(\theta_i, \phi_i)$ ,

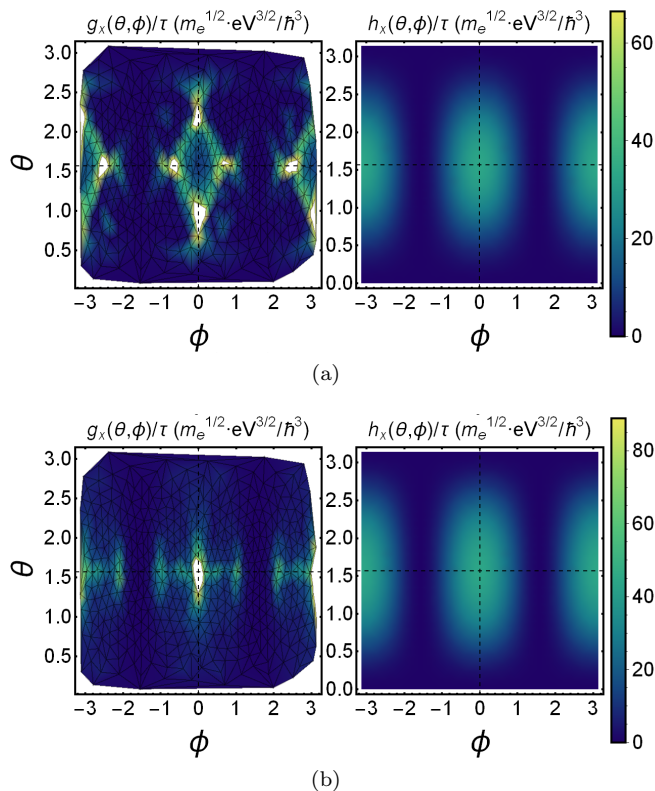


FIG. 7. The unaveraged values of  $g_x(\theta, \phi)$  (left) and the effective mass approximated  $h_x(\theta, \phi)$  (right) are shown for (a) Cu (b) [001]-textured Ru (in-plane averaging), assuming an isotropic bulk collision time and transport along  $v_t$  ( $\theta = \phi = \pi/4$ ) in case of Ru. Some outliers on the left are left out of the plot range for the sake of clarity.

equally spaced on the unit sphere. Examples of the resulting  $h_x(\theta, \phi)$  are shown in Fig. 7, next to the unaveraged  $g_x(\theta, \phi)$ . Even for Cu,  $g_x(\theta, \phi)$  does not seem to result from an isotropic Fermi surface. Nonetheless, the fitting results for Cu were found to be independent of the averaging procedure and to depend only on the assumption for bulk scattering (isotropy of collision time or mean free path).

Until now, we have always considered matching the bulk conductivity along the transport direction  $x$ , but one can also consider the out-of-plane conductivity  $\sigma_z^{\text{bulk}}$ , or the bulk conductivity  $\sigma_t^{\text{bulk}}$  along any direction  $t$ . The only change in the derivations above and in section II C consists of a replacement of the velocity squared that appears in the conductivity formula:  $v_{xn}^2 \rightarrow v_{tn}^2$ . Ideally, the resulting effective masses and Fermi energy should be compatible, but this does not appear to be the case

for Ru. Its nonellipsoidal multi-band Fermi surface lies at the heart of this inconsistency. The Fermi velocities of the complicated Fermi surface get projected to the velocity squared along the direction under consideration, a process which in general does not retain all the transport features, particularly in case of highly nonellipsoidal Fermi surfaces.

Fit	Transport	Isotropic	
		quantity	$M_{x,y}^2/M_z^2$
Fit	$v_x$	$\tau$	0.71
		$l_0$	0.69
	$v_z$	$\tau$	2.00
		$l_0$	2.51
	$v_t$	$\tau$	1.14
$(\theta = \phi = \pi/4)$	$l_0$	1.31	
Temperature		$\rho_{x-y}/\rho_z$	
Exp. [34]	100 K	1.33	
	200 K	1.32	
	300 K	1.31	
	400 K	1.29	

TABLE IV. The ratios of in-plane ( $\rho_{x-y}$ ) versus out-of-plane ( $\rho_z$ ) resistivity are listed for effective mass fits (given by  $M_{x,y}^2/M_z^2$ ) with different considerations of the transport velocity direction in Eq. (28), assuming an isotropic collision time or mean free path. Experimental values of the resistivity ratio are also presented for different temperatures.

We have fitted the effective masses based on a fitting procedure with bulk conductivities along different directions and the *ab initio* data presented in Fig. 3. When assuming a diagonal effective mass tensor, the ratio of in-plane versus out-of-plane resistivity, being an essential property of conduction band anisotropy, is proportional to  $M_{x,y}^2/M_z^2$ . The ratio obtained from the fit was found to be strongly dependent on the transport direction under consideration, as summarized in Table IV. When considering the in-plane and out-of-plane bulk conductivity, the obtained ratios do not agree with experimental results. Satisfactory agreement was obtained when considering transport along the  $(x = 1, y = 1, z = 1)$ -direction (or equivalently,  $\theta = \phi = \pi/4$ ), with an almost perfect match when assuming bulk scattering with isotropic mean free path. We suspect that a projection of the Fermi surface velocities on this transport direction optimally retains the essential transport properties. We have therefore adopted the effective mass fit with the consideration of  $v_t^2$  ( $\theta = \phi = \pi/4$ ) for the comparison with experimental data in section III.